Water Research 282 (2025) 123645

Contents lists available at ScienceDirect

Water Research

journal homepage: www.elsevier.com/locate/watres

Accurate detection and high throughput profiling of unknown PFAS transformation products for elucidating degradation pathways

Bei Zhang [a,b], Jibao Liu [c,*], Shanshan Qing [d], Thilini Maheshika Herath [c], Huan Zhao [a,b], Supaporn Klabklaydee [c], Qing-Long Fu [e], Eunsang Kwon [f], Nozomi Takeuchi [d], Douyan Wang [g], Takao Namihira [g], Toshihiro Isobe [h], Yanrong Zhang [i], Xiaoying Zhu [a,b], Baoliang Chen [a,b], Mohamed Ateia [j], Manabu Fujii [c,*]

[a] Department of Environmental Science, Zhejiang University, Hangzhou, Zhejiang 310058, China
[b] Innovation Center of Yangtze River Delta, Zhejiang University, Jiaxing, Zhejiang 314100, China
[c] Department of Civil and Environmental Engineering, Institute of Science Tokyo, Meguro-ku, Tokyo 152-8552, Japan
[d] Department of Electrical and Electronic Engineering, Institute of Science Tokyo, Meguro-ku, Tokyo 152-8552, Japan
[e] School of Environmental Studies, China University of Geosciences, Wuhan, Hubei 430074, China
[f] Research and Analytical Center for Giant Molecules, Graduate School of Science, Tohoku University, Sendai 980-8578, Japan
[g] Institute of Industrial Nanomaterials, Kumamoto University, Kumamoto 860-8555, Japan
[h] Department of Materials Science and Engineering, Institute of Science Tokyo, Meguro-ku, Tokyo 152-8552, Japan
[i] School of Environmental Science and Engineering, Huazhong University of Science and Technology, Wuhan, 430074, PR China
[j] Department of Chemical and Biomolecular Engineering, Rice University, Houston, TX, United States

ARTICLE INFO

Keywords:
PFAS homologues
Degradation pathways
FT-ICR MS
Paired mass distance networks
UV treatment
Plasma treatment

ABSTRACT

The accurate detection of unknown per- and polyfluoroalkyl substances (PFAS) transformation products (TPs) is essential for elucidating degradation pathways and advancing remediation strategies. Herein, we developed a workflow that combined Fourier transform ion cyclotron resonance mass spectrometry (FT-ICR MS) with a paired mass distance (PMD) network. This study achieved high throughput profiling of PFAS TPs with mDa resolving power and sub-ppm mass error. UV treatment revealed chain-shortening pathways, while plasma treatment uncovered competing mechanisms of chain shortening and lengthening, generating oxygen-rich TPs with increased hydrophilicity. Specifically, UV treatment of a 15-PFAS mixture and contaminated natural water showed disappearance of 7 unknown PFAS homologues and the emergence of 12 unknown PFAS homologues. Despite PFAS persistence under UV exposure, previously undetected low-abundance PFAS species were identified, indicating non-negligible photochemical transformation. Under plasma treatment of isolated PFOS, 39 unknown PFAS homologues including 142 suspect and 34 unknown PFAS TPs were identified, highlighting the extensive transformation of emerging and persistent PFAS. Overall, our approach enabled accurate and high-throughput profiling of unknown PFAS TPs and their degradation pathways, providing new insights into persistent unknown PFAS.

1. Introduction

Currently, over 7 million per- and polyfluoroalkyl substances (PFAS) are collected in "PubChem PFAS Tree" (Schymanski et al., 2023), including >10,000 PFAS that meet the OECD definition (Vestergren et al., 2024). During natural and engineering degradation processes, the proliferation of numerous transformation products (TPs) of PFAS is anticipated to escalate the number of unknown PFAS, including "known unknowns" that have not yet been reported in existing PFAS databases (Schymanski et al., 2014; Schymanski and Williams, 2017). Identification of these unknown PFAS TPs and mapping their degradation pathways are crucial to 1) make a fluorine mass balance, 2) assess potential risks and 3) guide the advanced remediation strategies for defluorination (Kempisty and Racz, 2021). However, existing analytical technologies face significant limitations. For instance, only <100 PFAS can be reliably detected by the current targeted analysis (Qiao et al., 2023;

* Corresponding authors.
E-mail addresses: liujibaoneu@163.com (J. Liu), fujii.m.ah@m.titech.ac.jp (M. Fujii).

https://doi.org/10.1016/j.watres.2025.123645
Received 9 January 2025; Received in revised form 29 March 2025; Accepted 12 April 2025
Available online 15 April 2025

Zweigle et al., 2023). Lack of reference standards makes it a great challenge in identifying and quantifying extensive unknown PFAS TPs (Wanzek et al., 2024) and their degradation pathways (Tang et al., 2023). Accurate detection is particularly challenging with unknown PFAS TPs in complex matrices with high concentration of background constituents (Singh et al., 2019; Zhu et al., 2019).

Nontargeted analysis (NTA) using high resolution mass spectrometry (HRMS) has been developed as a powerful tool to identify >1000 PFAS using time-of-flight mass spectrometry (TOF MS) and Orbitrap mass spectrometry (Orbitrap MS) (Bentel et al., 2019; Tang et al., 2023; X. Wang et al., 2024). Although technologies such as TOF MS and Orbitrap MS have advanced PFAS detection (X. Wang et al., 2024; Yu et al., 2018), collecting unconvoluted MS/MS spectra for low-abundance yet potentially important PFAS in complex matrices remains challenging (Young et al., 2022). In such cases, accurate detection of parent ion mass is essential for reliable identification. Additionally, existing *moderate-mass-error* screening (e.g., 5 ppm or 0.01 Da) often leads to false assignments of NOM and PFAS within mDa mass difference, requiring extensive screening via isotopologues, retention time, and MS/MS fragmentation approaches (Young et al., 2022). Nevertheless, in natural and engineered processes, unknown PFAS and their TPs usually occur with high chemodiversity, posing significant challenges to detect those at low abundance (Bentel et al., 2019; Singh et al., 2019). Consequently, many unknown PFAS TPs remain unidentified (Guan et al., 2024; Trang et al., 2022; Zhang et al., 2024), as evidenced by the missing fluorine-containing organics from fluorine mass balance studies (Dixit et al., 2024) during degradation processes (Singh et al., 2019). This limitation hinders the identification of low-abundance PFAS intermediates, many of which are critical to understanding degradation pathways and informing treatment designs.

Fourier transform ion cyclotron resonance mass spectrometry (FT-ICR MS) stands as the state-of-the-art HRMS, capable of resolving mDa mass difference and achieving sub-ppm mass error, allowing for precise detection of unknown PFAS TPs at low abundance (Dudášová et al., 2024; Zhou et al., 2023). Accurate mass measurements using FT-ICR MS have been well demonstrated to identify the molecular formulas for NOM and their byproducts (Dwinandha et al., 2023; Zhou et al., 2023). Notably, pioneering works have utilized FT-ICR MS to identify PFAS across various matrices, successfully resolving two classes of PFAS homologues with 59 mDa mass difference that other HRMS could not adequately resolve (D'Agostino and Mabury, 2014; Eeso et al., 2023; K. Li et al., 2023; Young et al., 2022; Zhu et al., 2019). By leveraging the ultrahigh mass resolution and accuracy of FT-ICR MS, it precisely detects the exact mass of unknown PFAS TPs for subsequent identification (Young et al., 2022). This capability unlocks the potential to resolve trace intermediates, and systematically explores PFAS degradation pathways with unprecedented detail.

A high-throughput profiling strategy is needed to elucidate degradation pathways of identified unknown PFAS TPs (Song et al., 2024). Since PFAS and their TPs usually occur as homologues (Young et al., 2022), CF_2-normalized Kendrick mass defect (KMD) has been employed to distinguish unknown PFAS homologues (Zhu et al., 2019). Young et al. visualized the connection of PFAS homologues via CF_2-based mass difference networks measured by FT-ICR MS (Young et al., 2022). However, significant challenges persist in effectively leveraging these CF_2 links from complex networks to explore unknown PFAS TPs and their degradation pathways. Paired mass distance (PMD) network advances the applicability of mass difference network in the field of metabolomics and NOM transformation (Dwinandha et al., 2023; Liu et al., 2023; X. Wang et al., 2024; Yu et al., 2019). The accurate mass of pairwise reactants and products measured by FT-ICR MS exhibits a unique mass difference, aligning with a predefined transformation reaction (L. Wang et al., 2024). Given the distinctive CF_2 units in PFAS structure and accurate mass measurement of FT-ICR MS, the application of PMD network alongside FT-ICR MS holds promise for high-throughput identification of unknown PFAS TPs and their degradation pathways, an area that has yet to be explored.

In this work, we developed a PMD-based workflow using FT-ICR MS to enable accurate identification of unknown PFAS TPs and provide actionable insights into their degradation pathways. Specifically, this study aims to bridge existing analytical gaps by systematically profiling PFAS TPs under UV treatment and plasma treatment processes. UV treatment was employed to simulate natural PFAS transformation processes in controlled laboratory conditions, while plasma treatment was utilized to investigate engineered degradation pathways. Benefiting from the accurate mass measurement of FT-ICR MS using samples before and after treatment, our workflow enables *low-mass-error* (mass error < 0.5 ppm) and high-throughput profiling of PFAS TPs as homologues using their exact CF_2 mass difference (49.99681n Da). This allows to visualize disappeared, reserved, and generated PFAS homologues during treatment processes. The findings from this study are poised to advance not only PFAS detection methodologies for environmental samples but also inform the development of scalable treatment strategies tailored to mitigate PFAS and TPs.

2. Materials and methods

2.1. Preparation of PFAS samples under UV treatment and plasma treatment

Targeted treatment processes mimic conditions relevant to environmental remediation systems, providing insights into degradation under natural and engineered scenarios. Details regarding the preparation of PFAS samples are provided in the Supporting Information (Text S1-S3 and Table S1). Briefly, standards of 15 PFAS were purchased to prepare the PFAS mixture (PFAS-M) including: Perfluorooctanesulfonic acid (PFOS) homologues (C_4-C_8), perfluorooctanoic acid (PFOA) homologues (C_4-C_8), and perfluorooctanesulfonamide (FOSA) homologues (C_4-C_8). Natural water samples were collected at four sites from upstream (NW-1) and downstream (NW-2, NW-3 and NW-4) of a suspiciously PFAS-contaminated river in Japan (Text S2 and Table S2). UV treatment of PFAS mixture (PFAS-M-UV) and natural water samples (NW-2-UV) was conducted to investigate natural transformation of PFAS.

Next, plasma treatment was employed to investigate engineering degradation pathways of PFAS. Specifically, around 5 mg/L of PFOS was gradually decomposed under a pulsed gas-liquid discharge nonthermal plasma reactor with a pulsed power supply (Wang et al., 2022) (Text S3). The initial PFOS sample and degradation samples at 15 min (Plasma-15 min), 30 min (Plasma-30 min) and 60 min (Plasma-60 min) during plasma treatment were collected for measurement of the concentration of F^- (Text S3). Solid phase extraction (SPE) treatment of untreated, UV-treated and plasma-treated samples was subsequently operated (Text S2 and S3) for further FT-ICR MS and LC-MS/MS measurements (Taniyasu et al., 2008). The variation in treatment and SPE conditions was necessitated by the distinct characteristics of PFAS TPs generated under UV and plasma treatments (discussed in Text S3). It should be acknowledged that only anionic PFAS were analyzed in this study, as dictated by the selected SPE procedures and the operating modes of FT-ICR MS and LC-MS/MS.

2.2. FT-ICR MS measurement

PFAS samples were filtered using 0.22 μm well-rinsed cellulose acetate membrane for FT-ICR MS measurement in electrospray ionization (ESI) negative mode (12 T, SolariX XR, Bruker, Germany). The FT-ICR MS instrumental conditions were provided in the Supporting Information (Text S4). The FT-ICR MS instrument was externally calibrated using sodium formate solution, and the mass spectra were internally recalibrated using a home-built PFAS reference mass over the entire mass range (Zhu et al., 2019).

2.3. PMD network screening workflow

The PMD-based workflow is illustrated in Fig. 1. Detailed instructions for using the web tool, along with a video tutorial, are provided in Text S5. As shown in Figure 1a and S1c, PFAS identification confidence was annotated to the relevant screening results in the workflow. The schematic illustration was also provided in Fig. 1c to visualize the screening processes. Based on the mass lists from FT-ICR MS, the strategy of PMD network was applied to identify and visualize homologous PFAS series based on precise mass differences, providing a systematic framework for detecting transformation pathways (Fig. 1b). This network-based approach is not limited to FT-ICR MS and can be adapted for use with Orbitrap MS or TOF MS, making it accessible to a broader scientific community.

1) PFAS homologue screening: All peaks in the mass list from each sample were utilized to calculate their mass differences with the other peaks. If the mass error of calculated mass differences compared to exact mass of $(CF_2)_n$ (times of 49.99681 Da) is <0.5 ppm, the paired mass was assigned as nodes (level 5) connected by $(CF_2)_n$ links (or edges) (Fig. 1c). The connected nodes and links potentially consist of diverse modules as tentative PFAS homologues for each sample with the number of nodes showing the size of modules. According to refined classification (Charbonnet et al., 2022; Young et al., 2022) and our definition of PFAS identification confidence, we consider that fully connected modules (i.e., complete graph, where all nodes are connected with each other as shown in Fig. 1c) possess higher identification confidence, exhibiting higher priority for suspect and targeted analysis (level 5 to level 1).

2) Suspect screening: Suspect screening of all peaks in the mass list was conducted to facilitate a high-throughput identification of PFAS homologues. An extensive PFAS suspect list containing over 200,000 known and unknown PFAS from National Institute of Standards and Technology (NIST), Norman, and U.S. Environmental Protection Agency (US EPA), and PFAS in PubChem Tree (details in Text S5). Chemical information was assigned to the observed peaks by suspect screening when masses matched. Importantly, even though unassigned peaks during suspect screening exist in PFAS homologues containing assigned peaks, their formula can be indirectly assigned as PFAS homologues (at level 5 to level 4, Fig. 1c). If multiple formulas were assigned to one mass peak during suspect screening, unequivocal formulas can be extracted by using information from the same PFAS homologues (at level 5 to level 4 or 3). Therefore, the integration of suspect and network screening substantially facilitates the formula assignment of modules containing suspect PFAS for further identification. In terms of tentative PFAS homologues without assigned formula, batch formula assignment was performed using a home-built database of F-containing formulas (details in Text S5).

3) Target analysis: The 15 PFAS standards were applied to develop the target analysis (level 1) method using LC-MS/MS (LCMS-8050, Shimadzu, Japan) with an electrospray ionization (ESI) in negative ion mode (Text S6). Accordingly, the concentrations of target PFAS in natural water samples and treated samples were measured as shown in Supporting Information (Text S6, Table S3 and Table S4). In this work, some representative peaks (high-degree nodes in PFAS homologues network) in natural water samples and degradation samples were analyzed by MS/MS fragmentation (Text S7). Ultrapure water was used as procedural blanks to monitor background contamination. Procedural recoveries were detected in the range of 90 % to 110 %. Regarding quality control and quality assurance (QA/QC), nine-point calibration in the range of 10 to 5000 ng/L was used for quantification. Limits of detection (LOD) was determined to be 0.1 ng/L based on pretreatment and measurement procedures. To account for potential matrix effects, matrix-matched standards (using natural organic matter matrix for natural water samples and plasma blank samples) were analyzed. No PFAS were detected in these matrix-matched standards. Additionally validation using internal standard was performed, as detailed in Text S6.

4) Multi-layer network: To further analyze the transformation of PFAS homologues, the $(CF_2)_n$-based PMD network approach was extended based on PMD-based reactomics for NTA of metabolomics (Yu

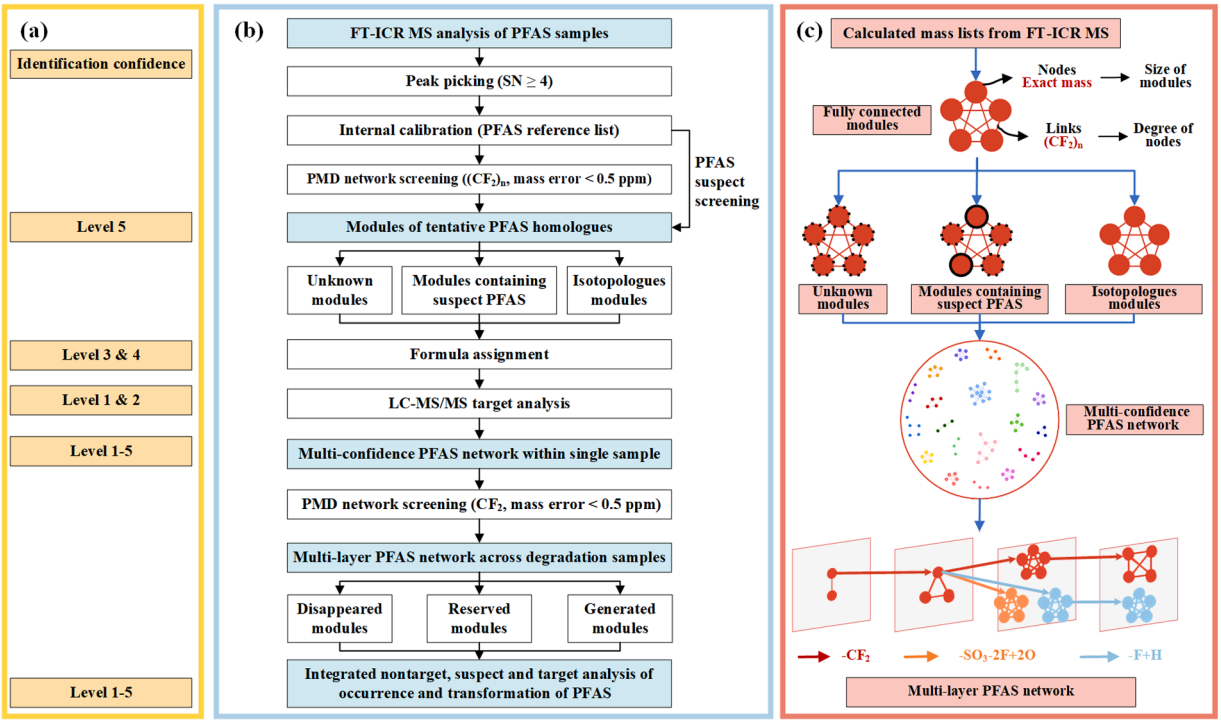

Fig. 1. (a) Annotation of PFAS identification confidence related to screening results; Integrated workflow (b) and schematic illustration of network parameters (e.g., nodes, links, modules) and screening processes for the generation of multi-confidence PFAS networks and multi-layer PFAS networks (c). Identification confidence increases from exact mass of interest (level 5) to unequivocal molecular formula (level 4), tentative candidates (level 3), probable structure (level 2), and confirmed structure (level 1).

and Petrick, 2020). To validate this hypothesis, CF_2 network screening was applied to the treated samples (i.e., PFAS-M and PFAS-M-UV, NW-2 and NW-2-UV, and plasma-treated PFOS samples). Eventually, multi-layer networks consisting of multi-confidence PFAS networks hierarchically connected by CF_2 links were established to visualize the potential transformation of PFAS species under treatment processes (Fig. 1c and Text S5) (Kokoli et al., 2023).Three types of modules were identified including disappeared modules (the modules only found before treatment), reserved modules (modules found both before and after treatment, and the module size after treatment may be identical, smaller, or larger), and generated modules (new modules after treatment) (Fig. 1b). The expanded comparison of various PFAS homologues before and after treatment processes was conducted to explore the transformation process by using various links (e.g., -SO_3/+2HO-2HF related to degradation of PFOS into PFOA, -F + H related to H/F exchange, see details in Section 3).

5) Theoretical calculation: In terms of high-abundance TPs of PFOS under plasma treatment, their available structures in PubChem and C-F bond dissociation energies (BDEs) were examined by density functional theory (DFT) simulation using reported methods (details in Text S8).

3. Results and discussion

3.1. High-resolution detection and PFAS profiling

The combination of FT-ICR MS and a PMD-based workflow enables precise PFAS profiling, resolving complex mixtures and identifying low-abundance TPs with high accuracy. The calibrated FT-ICR MS spectra labeled with 15 PFAS and their LC-MS/MS spectra were provided in Figure S1. Using a PFAS reference mass for internal calibration, FT-ICR MS achieved narrow mass errors ranging from -0.016 to 0.024 ppm across 15 PFAS standards (Table S5). For short-chain PFAS, mass errors of PFBS, PFBA, and FBSA were calculated as 0.004 ppm, 0.001 ppm and 0.009 ppm, respectively. A precise mass difference screening (mass error $<$ 0.5 ppm) was then conducted to generate a tentative PFAS homologues network (Fig. 2a and Figure S3).

Based on refined identification confidence (Charbonnet et al., 2022; Young et al., 2022), seven fully connected modules (each containing 5 nodes) were firstly identified as marked in Fig. 2a. Integrating with suspect screening, all 15 PFAS were tentatively assigned in 3 fully connected modules with their ^{13}C and ^{34}S isotopologues in other 4 fully connected modules. Each module was verified through formula assignment and LC-MS/MS validation, demonstrating the robustness and reliability of the approach (Figure S2a-c). The interactive networks in HTML format (PFAS-M) and screening results in Excel files (detailed information of modules and assigned formula in sheets) can be accessed in Text S5.

The connection of nodes within the same module can facilitate the screening of homologue formulas (Fig. 2b). Specifically, two formulas of $C_{10}H_5Cl_2F_5N_2S$ and $C_5HF_{11}O_3S$ were assigned to the detected mass (i.e., 348.939797 Da) by suspect screening. Furthermore, the formula of $C_5HF_{11}O_3S$ as another homologue node in this module was confirmed by low mass error of -0.0029 ppm and LC-MS/MS with PFPeS standard. This screening approach was also proved in PFOA modules (Figure S4a) and FOSA modules (Figure S4b) to facilitate the final validation by LC-MS/MS.

Another 12 emerging and unknown modules were identified in PFAS-M (Fig. 2a and Figure S5). Notably, a fully connected module with 11 nodes and its isotopologues modules (marked as unknown homologues in Fig. 2a and Figure S5a) were assigned to $C_8H_3O_4NSF_{16}$ homologues (C_6-C_{16}) by suspect screening and homologues assignment (Figure S6a). Only $C_{11}H_3O_4NSF_{22}$ was found in PubChem, with no reported information available for other homologues. Nevertheless, all formulas of $C_8H_3O_4NSF_{16}$ homologues were confirmed in subsequent batch formula assignment (marked in the sheet of UME-PFAS-M in attached Excel file in Text S5), showing consistent results across suspect screening, homologues assignment and batch formula assignment. The generation of $C_8H_3O_4NSF_{16}$ homologues was ascribed to the adduct or complex among PFOA, PFOS and FOSA homologues. Notably, the transformation among N-ethyl perfluorooctane sulfonamidoethanol (N-EtFOSE, $C_{12}H_{10}F_{17}NO_3S$), PFOA and FOSA has been reported (Nguyen et al., 2013), as further validated in Section 3.2.

3.2. PFAS transformation pathways under UV treatment

UV treatment revealed significant transformation of known PFAS into diverse unknown TPs, highlighting previously uncharacterized pathways critical for understanding PFAS degradation dynamics (Fig. 2 and 3). For the PFAS-M sample, UV treatment resulted in the disappearance of 5 homologues, retention of 13 homologues, and generation of 10 new homologues, forming the basis for mapping their transformation pathways (Fig. 3c and 3d, all modules in Figure S7). Specifically, $C_8H_4F_{12}O_3$ homologues (C_6-C_{10}) and $C_9F_{21}N_1O_2S_1$ homologues (C_9-C_{14}) in Fig. 3d, potentially derived from PFOA homologues (+3H-3F-O for their formula difference) and FOSA homologues (+C-2H+4F), disappeared after UV treatment, tentatively classified as unstable PFAS homologues. In contrast, two generated modules (i.e., $C_8H_3F_{13}O_4$ (C_5-C_9) and $C_8HF_{18}NO_2S$ (C_5-C_9) in Fig. 3d) were designated as TPs of PFAS-M, potentially derived from PFOA homologues (+2H-2F+2O) and FOSA homologues (-H + F), respectively.

Three modules containing 15 PFAS, newly identified $C_8H_3O_4NSF_{16}$ homologues (C_6-C_{16}, Figure S6b), and C_4HF_9 homologues (C_4-C_7, Figure S6b) were preserved (Fig. 3c and 3d) after UV treatment of PFAS-M, indicating high stability of PFAS against UV treatment. The most abundant PFAS during UV treatment was changed from PFOS (100 % to 88 % in relative abundance) to PFHxS (87 % to 100 % in relative abundance), suggesting a potential chain shortening transformation among 15 PFAS. Bentel et al. identified the chain shortening transformation (decarboxylation-hydroxylation-elimination-hydrolysis, DHEH pathway) among PFOA and PFOS homologues under attacked by hydrated electrons (Bentel et al., 2019). Short-chain PFAS TPs (e.g., PFHpA, PFHxA, PFPeA, PFBA, PFPrA, and TFA) were also confirmed by reported pathways under UV treatment (Z.G. Li et al., 2023). Additionally, the abundance of $C_8H_3O_4NSF_{16}$ homologues was significantly decreased with increasing abundance of FOSA homologues (C_4-C_8), indicating a potential transformation between $C_8H_3O_4NSF_{16}$ homologues (C_6-C_{16}) and FOSA homologues (C_4-C_8). Notably, two unknown modules in Fig. 3d are not found in the suspect list, suggesting that further efforts are needed to identify these unknown PFAS. However, their low abundance and unknown information pose a significant challenge for current HRMS technologies. Nevertheless, their tentative PFAS formulas were provided in different modules (Excel files in Text S5) for further analysis when conditions permit.

Natural transformation of PFAS was investigated by identified PFAS homologues before and after UV treatment. The module of PFBS and PFOS was found in upstream NW-1 (Fig. 3a), as detected by LC-MS/MS analysis (5.4 ng/L of PFBS and 19.4 ng/L PFOS in Table S3), indicating potential contamination in source river in Japan. Three modules of PFOA homologues (C_5-C_9), PFOS homologues (C_2-C_8), FOSA homologues (C_3-C_6) were found in downstream samples (i.e., NW-2, NW-3 and NW-4 in Fig. 3a), consistent with quantitative results using LC-MS/MS (Fig. 3b and Table S3). Notably, ultrashort-chain PFAS (i.e., $C_2HF_5O_3S$, $C_3HF_7O_3S$, and $C_3H_2F_7NO_2S$) were identified in NW-2 (Fig. 3a). While their linear structures, including pentafluoroethanesulfonic acid (PFEtS), perfluoropropanesulfonic acid (PFPrS), and perfluoropropane sulfonamide (FPrSA), and isomers could be quantitively verified with their reference standards, our network screening detected these low-abundance peaks connected with their PFAS homologues, suggesting their potential presence in NW-2.

The potential transformation of PFAS homologues across downstream samples (i.e., NW-2 to NW-3 and NW-4) was visualized by multi-layer network (Fig. 3c and detailed modules in Figure S8) and

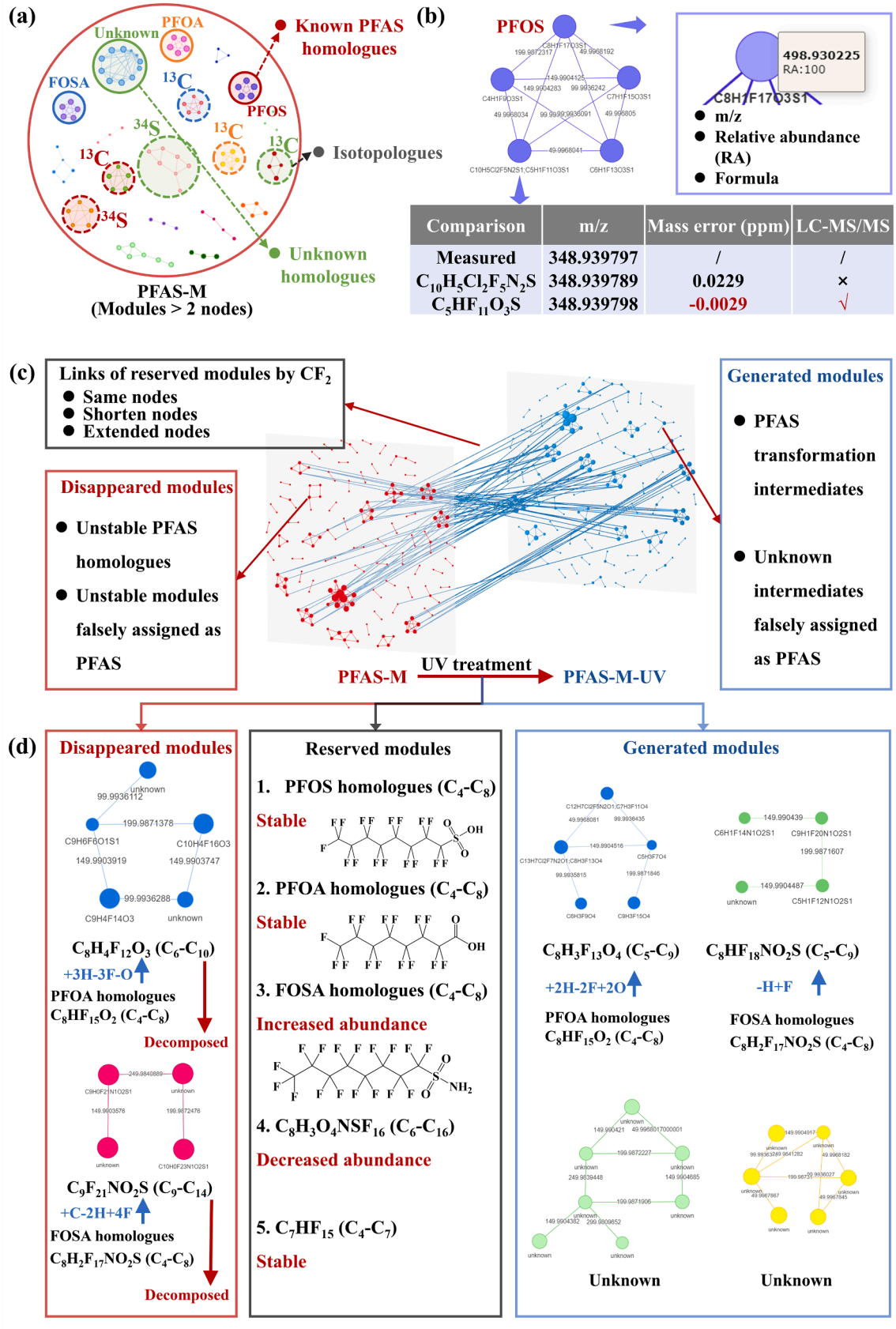

(caption on next page)

Fig. 2. Network screening of 15 PFAS mixture under UV treatment: (a) Modules containing more than two nodes classified as "known PFAS homologues" (containing known 15 PFAS), "isotopologues modules" (containing isotopologues of 15 known PFAS), and "unknown homologues" (marked modules: 7 fully connected modules with 5 nodes including 3 modules of PFAS homologues (C_4-C_8) and 4 isotopologues modules, and one fully connected module with 11 nodes and its isotopologues modules); (b) Tentative PFOS modules (C_4-C_8, including *m/z*, relative abundance (RA), formula, and mass difference) and subsequent identification of PFPeS ($C_5HF_{11}O_3S$) (i.e., two formulas $C_{10}H_5Cl_2F_5N_2S$ and $C_5HF_{11}O_3S$ were assigned by suspect screening, and the formula of $C_5HF_{11}O_3S$ was selected by low mass error of −0.0029 ppm and PFOS homologues assignment and finally validated by and LC-MS/MS with PFPeS standard); (c) Multi-layer network of PFAS-M before and after UV treatment (modules across two samples were classified as three types including disappeared modules, reserved modules connected by CF_2 links, and generated modules); (d) detailed information of three types of modules and potential transformation during UV treatment.

quantitative analyzed by LC-MS/MS (Fig. 3b and Table S3). Accordingly, same-type modules of PFOA, PFOS, and FOSA homologues were found in NW-2 and NW-3. However, long-chain PFAS (i.e., $C_9HF_{17}O_2$) were absent in NW-4, which may be ascribed to photolysis or physical removal (e.g., adsorption or complexation) during migration processes.

The photolysis of long-chain PFAS was verified by the UV treatment of NW-2 (Fig. 3d and Figure S9). Additionally, two short-chain PFOA homologues (i.e., $C_3HF_5O_2$ and $C_4HF_7O_2$) were identified for NW-2 with UV treatment (Fig. 3d and Figure S9). A total of 40 unknown modules containing more than two nodes were found in NW-2 before and after UV treatment (Excel file in Text S5). These modules could be potentially unknown PFAS homologues (batch formula in Excel file in Text S5) or NOM falsely assigned as PFAS. Different reactivities of PFAS and NOM under UV treatment help to screen false assignment, in which unstable NOM tends to be decomposed under UV treatment based on our reports (Dwinandha et al., 2023). While the low abundance and limited information about TPs of PFAS present substantial challenges for current HRMS technologies, our workflow enables efficient screening of these peaks, laying the groundwork for subsequent validation in the future.

3.3. PFAS degradation pathways under plasma treatment

Plasma treatment facilitated extensive PFOS decomposition, revealing novel degradation pathways involving both chain-shortening and chain-lengthening mechanisms. As shown in Fig. 4a, hundreds of tentative TPs of PFOS were identified in the multi-layer network, indicating the formation of diverse TPs at the plasma-gas-liquid interface (Figure S10, S11 and Fig. 4). This was induced by high-energy particles, localized high temperature, and reductive (e.g., hydrated electrons, argon ions, and hot electrons) and oxidative (e.g., $SO_4^{\bullet-}$ and $^{\bullet}OH$) species produced from the discharge process. The number of total modules significantly increased from 7 (PFAS impurities in the initial PFOS) to 102 (Plasma-15 min), 116 (Plasma-30 min), and 110 (Plasma-60 min) (Fig. 4b). Most modules with more than two nodes (e.g., 36 out of 39 modules at 30 min) contain at least one suspect PFAS (Fig. 4b). These modules containing suspect PFAS (details in attached Excel file in Text S5) serve to propose an elaborate transformation pathway (as discussed below) based on the extensive collection of over 200,000 PFAS in the suspect list. Additionally, 13 unknown modules and 40 unknown nodes after plasma treatment (Fig. 4b and 4c) were detected as unknown PFAS candidates. To the best of our knowledge, these PFAS formulas have not been reported elsewhere (attached Excel files in Text S5).

Based on available references standards of PFOS homologues and PFOA homologues, the occurrence and transformation of PFOS toward PFOA support the reported chain-shortening pathway (illustrated in Fig. 4c, 4d and Figure S12). The observed distribution of PFOS and PFOA homologues network across treatment processes showed high consistency between their concentration analyzed by target analysis (Table S4 and Figure S13) and RA detected from FT-ICR MS (Table S6 and Figure S13), suggesting a potential semi-quantitative analysis using HRMS under designed conditions.

Pioneering works have been conducted using HRMS for NTA of emerging and unknown TPs (Bentel et al., 2019; Singh et al., 2019). However, current limitations, including experience-based screening (Tachibana et al., 2014), large mass error (Bentel et al., 2019; Singh et al., 2019), and limited dataset (Bentel et al., 2019), restrict the exploration of extensive TPs via NTA approach. For example, *m/z* at 395 obtained from plasma treatment of PFOS has been assigned to $C_8H_2F_{14}O_2$ based on a reported screening (Tachibana et al., 2014). However, based on our detected *m/z* of 394.9452871 using FT-ICR MS, $C_6H_3F_{11}O_5S$ was assigned in a fully connected module (No. 1 homologues in Fig. 4e). Additionally, a lower mass error of detected *m/z* of 394.9452871 for $C_6H_3F_{11}O_5S$ (0.023 ppm) was achieved in comparison to that of $C_8H_2F_{14}O_2$ (-77.372 ppm). The occurrence of $C_6H_3F_{11}O_5S$ and its long-chain homologues (i.e., $C_7H_3F_{13}O_5S$ and $C_8H_3F_{15}O_5S$) was also identified as TPs of PFOS under plasma treatment. Notably, two short-chain homologues, including $C_4H_3F_7O_5S$ and $C_5H_3F_9O_5S$, in low abundance were identified in this work as potential TPs of PFOS for the first time.

Utilizing our NTA approach, a total of 37 reported (known and known unknowns) and 53 novel (unreported unknowns) TPs of PFOS with an abundance higher than 1 % were identified as shown in Table S7. After 30 min of plasma treatment, the most extensive TPs, including 14 reported and 30 novel TPs, were identified. To obtain chromatographic information of these TPs, LC-MS measurement in SIM mode was conducted using the *m/z* value of TPs detected in FT-ICR MS measurement. The RSpak JJ-50 column was utilized, where PFAS with more hydrophilic nature tend to have longer retention time via ion exchange interaction (details in Text S6). Among these 30 novel TPs, 21 TPs possess longer retention time than PFOS (13.5 min). Hydrophilic short-chain PFAS are known to be persist under plasma treatment due to their limited accumulation at the plasma-gas-liquid interface, making them less likely to be decomposed by reactive species. However, emerging and unknown hydrophilic TPs of PFOS are rarely identified, to the best of our knowledge. Most importantly, identifying these TPs, which escape robust plasma treatment and persist in aqueous solution, is essential for assessing residual PFAS and water quality post-treatment. Subsequent efforts can focus on upgrading plasma treatment technology to achieve complete defluorination.

To clarify potential transformation from PFOS to emerging and unknown hydrophilic TPs identified in this work, C-F bond dissociation energies (BDEs) of PFOS were calculated as shown in Fig. 4e and attached Excel file in Text S5. Compared to terminal C-F bond (-CF_3, 118.7 kcal mol^{-1} of BDE), middle-chain C-F bonds with low BDEs (-CF_2-, 104.4-106.5 kcal mol^{-1} of BDE) are susceptible to cleavage when reacting with e_{aq}^- generated during plasma treatment. Consistent with increasing hydrophilicity of TPs, oxygen-rich TPs were identified in high abundance across 12 modules (Table S8). Reactive oxygen species (ROS), such as $^{\bullet}OH$, were presumed to react with TPs reduced by e_{aq}^-. Eventually, the integration of reductive e_{aq}^- and ROS could enhance the decomposition of PFOS in aqueous solution.

Based on exact mass measurement and our NTA approach, potential transformation of PFOS into C_8 TPs was illustrated in Fig. 4e. Initial reduction of PFOS by e_{aq}^- achieved gradually defluorination via H/F exchange processes, generating $C_8H_2F_{16}O_3S$ (No.6 homologues in Table S8), $C_8H_3F_{15}O_3S$ (measured in Table S7), $C_8H_4F_{14}O_3S$ and $C_8H_5F_{13}O_3S$ (proposed in this work). Subsequent OH abstraction induced by ROS produced hydrophilic TPs, including $C_8H_3F_{15}O_4S$ (No.8), $C_8H_3F_{15}O_5S$ (No.1), $C_8H_4F_{14}O_4S$ (No.3), $C_8H_4F_{14}O_5S$ (No.7), $C_8H_5F_{13}O_5S$ (No.2). However, available structures of these TPs (i.e., $C_8H_3F_{15}O_4S$ and $C_8H_3F_{15}O_5S$) in PubChem possess ether units, which contribute less to increasing hydrophilicity. In contrast, hydroxylated TPs generated from OH abstraction significantly increased hydrophilicity. Hydroxylated TPs (or alcohol TPs) have been proposed to clarify

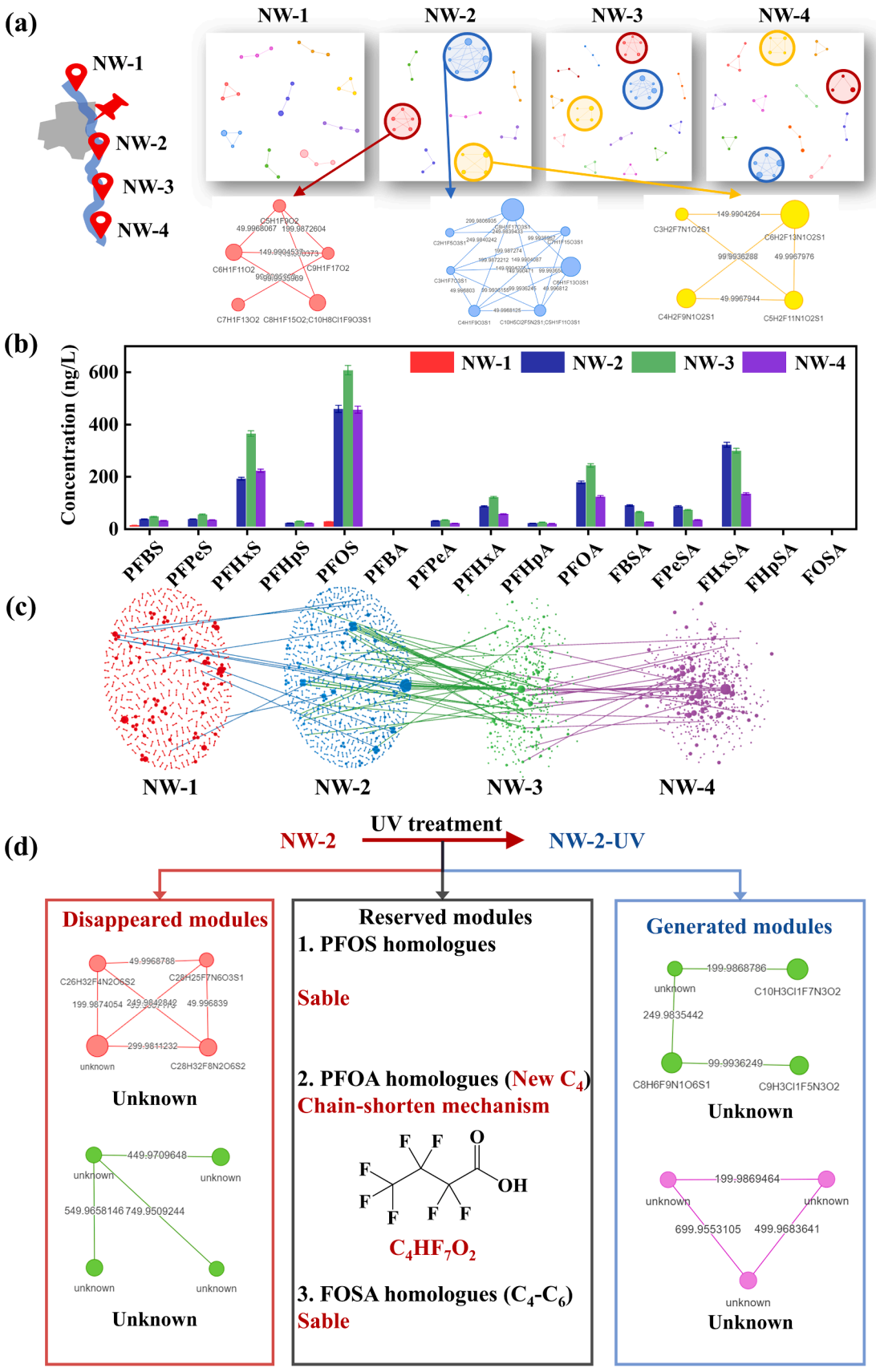

Fig. 3. (a) Sampling information (left), modules containing more than two nodes in samples of NW-1, NW-2, NW-3 and NW-4 (top right), and detailed information of PFOA modules (C_5-C_9), PFOS modules (C_2-C_8) and FOSA modules (C_3-C_6) in NW-2 (bottom right); (b) Concentration of PFOA modules (C_4-C_8), PFOS modules (C_4-C_8) and FOSA modules (C_4-C_8) for NW-1, NW-2, NW-3 and NW-4; (c) Multi-layer network of NW-1, NW-2, NW-3 and NW-4 connected by CF_2 links; (d) Detailed information of disappeared modules, reserved modules, and generated modules of NW-2 during UV treatment.

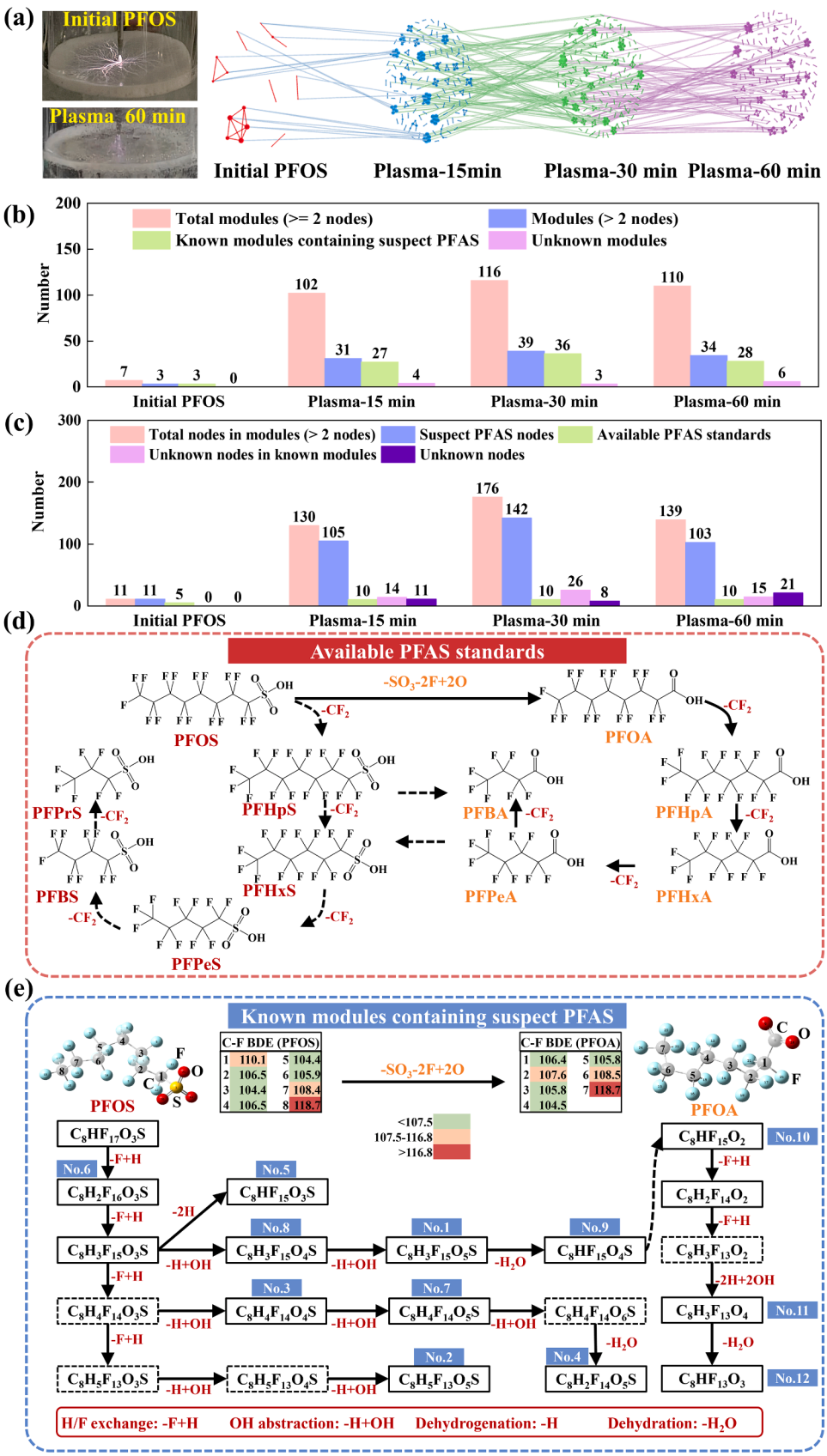

(caption on next page)

Fig. 4. (a) Photos of plasma treatment at initial stage and 60 min (left) and multi-layer network (right) of initial PFOS, Plasma-15 min, Plasma-30 min and Plasma-60 min connected by CF_2 links; (b) Quantitative analysis of distribution of identified modules in the multi-layer network across plasma treatment; (c) Quantitative analysis of distribution of identified nodes in the modules containing more than two nodes; (d) Validated transformation from PFOS to PFOA (-SO_3–2F+2O) and subsequent shorten-chain transformation (-CF_2) utilizing identified known PFAS; (e) Extended transformation from PFOS to PFOA and their TPs existed in modules containing suspect PFAS (No.1–9 in solid line boxes) and theoretical TPs (in dashed line boxes), including potential reactions (i.e., H/F exchange, OH abstraction, dehydrogenation, and dehydration).

oxidative pathways of PFAS (Liu et al., 2021). Here, we provided experimental detection and identification of hydroxylated TPs, including their exact mass, retention time and homologues in Table S7.

Following H/F exchange and OH abstraction, dehydrogenation and dehydration processes generated pyruvate TPs such as $C_8HF_{15}O_3S$ (No.5), $C_8HF_{15}O_4S$ (No.9), and $C_8H_2F_{14}O_5S$ (No.4), which are supposed to lead to the formation of carboxylic TPs (e.g., PFOA. The transformation of PFOS to PFOA have been well investigated in reported works (Singh et al., 2019; Tachibana et al., 2014; Takeuchi et al., 2014). In this work, after H/F exchange of PFOA, their hydroxylated and pyruvate TPs were identified, including $C_8H_3F_{13}O_4$ (No.11) and $C_8HF_{13}O_3$ (No.12). All 12 C_8 TPs were included in the proposed transformation pathway (Fig. 4e). Notably, the degradation pathways shown in Fig. 4e can be theoretically validated through DFT calculations to optimize the potential structures of TPs, which is currently under investigation in our ongoing research. Nevertheless, structural annotation for each identified unknown PFAS would require integrating our workflow with advanced MS/MS fragmentation techniques, which falls beyond the scope of this study.

In addition to short-chain TPs potentially formed via chain-shortening mechanisms, long-chain TPs (C_9-C_{16}) were identified as shown in Table S8. A chain-lengthening process has been reported to explain the formation of long-chain PFAS during biomimetic degradation (Li et al., 2020). However, long-chain TPs of PFAS were rarely reported in other systems. Perfluoroalkyl radicals have been well reported as reactive intermediates during degradation of PFOS (Bentel et al., 2019). Accordingly, perfluoroalkyl radical polymerization and the addition of these perfluoroalkyl radicals with weak C-H or C-OH bonds in TPs (Fig. 4e) were proposed to lead to the formation of long-chain TPs. Accordingly, non-linear TPs would be generated for chain-lengthening mechanisms. However, the relatively low abundance of long-chain TPs detected in this work (mainly < 0.1 % in attached Excel file in Text S5) indicates that chain-lengthening mechanisms are not a primary transformation pathway under plasma treatment.

Due to single PFOS precursor and robust plasma treatment, fewer unknown modules without assignment of suspect PFAS (Figure S14) were identified compared to those of mixed PFAS and natural samples in Section 3.1 and 3.2. Tentative formulas of these unknown TPs were provided in the attached Excel file (Text S5) for structural identification. Nonetheless, structural annotation of emerging and unknown TPs remains limited using open datasets and reported NTA approaches. For example, structures of $C_8H_3F_{15}O_5S$ homologues (No.1 in Fig. 4e) in PubChem have no identical core structures and repeating CF_2 units, which contradicts the chain-shorten mechanism within homologues. Additionally, collecting unconvoluted MS/MS spectra for these low-abundance TPs remains challenging when applying reported NTA approaches. Further exploration of our developed platform with HRMS is essential for structural identification as conditions permit in the future.

4. Conclusions

In this work, accurate mass measurement of PFAS using FT-ICR MS, combined with the PMD strategy, achieves precise and high-throughput acquisition of mass differences among known and unknown PFAS homologues. Accordingly, extending PMD to treated samples elucidates potential transformation based on disappeared, reserved, and generated modules. Importantly, we demonstrate the persistence of PFAS under UV treatment compared to plasma treatment. Our screening approach identified low-abundance PFAS TPs generated during UV treatment. Although the abundance of these TPs is low, their widespread distribution and potential accumulation in natural transformation processes cannot be overlooked. Furthermore, plasma treatment proves more feasible for high-concentration PFAS following concentration processes (e.g., membrane filtration or foam fractionation), given its removal efficiency and energy efficiency. However, hydrophilic TPs may evade treatment even with high removal efficiency. Therefore, both known and unknown PFAS TPs must be carefully considered and assessed in scalable treatment processes. Advanced workflows based on direct infusion FT-ICR MS measurement (e.g., PFlow (Dudášová et al., 2024)) and MS/MS fragmentation(e.g., FindPFΔS (Zweigle et al., 2022), FluoroMatch (Koelmel et al., 2022), and APP-ID (X. Wang et al., 2024)) could be integrated for further screening and structural annotation of emerging and unknown PFAS. To comprehensively understand the PFAS transformation behavior in the natural and engineered system, increased attention and effort will be valuable on the PFAS non-target analysis using HRMS and algorithms that combine experimental and theoretical approaches.

CRediT authorship contribution statement

Bei Zhang: Writing – original draft, Visualization, Supervision, Methodology, Investigation, Funding acquisition, Data curation, Conceptualization. **Jibao Liu:** Writing – review & editing, Supervision, Methodology, Investigation, Conceptualization. **Shanshan Qing:** Writing – review & editing, Methodology, Investigation. **Thilini Maheshika Herath:** Writing – review & editing, Methodology, Investigation. **Huan Zhao:** Writing – review & editing, Methodology, Investigation. **Supaporn Klabklaydee:** Writing – review & editing, Methodology, Investigation. **Qing-Long Fu:** Writing – review & editing, Investigation. **Eunsang Kwon:** Writing – review & editing, Resources, Methodology. **Nozomi Takeuchi:** Writing – review & editing, Resources, Methodology. **Douyan Wang:** Writing – review & editing, Resources, Methodology. **Takao Namihira:** Writing – review & editing, Resources, Methodology. **Toshihiro Isobe:** Writing – review & editing, Resources, Investigation, Funding acquisition. **Yanrong Zhang:** Writing – review & editing. **Xiaoying Zhu:** Writing – review & editing, Methodology, Investigation. **Baoliang Chen:** Writing – review & editing, Methodology, Investigation. **Mohamed Ateia:** Writing – review & editing. **Manabu Fujii:** Writing – review & editing, Supervision, Methodology, Funding acquisition.

Declaration of competing interest

The authors declare that they have no known competing financial interests or personal relationships that could have appeared to influence the work reported in this paper.

Acknowledgments

This study was financially supported by the Provincial “Leading Goose” Key Technology Research and Development Program of Zhejiang, China (2025C02229), the National Natural Science Foundation of China (U24A20522), Foreign Specialist Program (H20240372), JSPS Kakenhi (20F20044, 22H01623, 23KK0074 and 24K17381), DLab Challenge Research Grant, and Joint Research by the Institute of Industrial Nanomaterials, Kumamoto University. This work was partially

supported by collaborative research between Institute of Science Tokyo and National Institute of Advanced Industrial Science and Technology (AIST). The authors would like to thank Dr. Sachi Taniyasu and Dr. Nobuyoshi Yamashita in AIST for their advice on SPE treatment. The authors appreciate the technical support from Hiroyuki Momma in FT-ICR MS measurement and members from Fujii lab on the sampling and data analysis. Bei Zhang thank the discussion from Bao Zhu on the internal calibration. This work utilized TSUBAME supercomputers that operate at the GSIC Center at the Institute of Science Tokyo, Japan.

Supplementary materials

Supplementary material associated with this article can be found, in the online version, at doi:10.1016/j.watres.2025.123645.

Data availability

Data will be made available on request.

References

Bentel, M.J., et al., 2019. Defluorination of per- and polyfluoroalkyl substances (PFASs) with hydrated electrons: structural dependence and implications to PFAS remediation and management. Environ. Sci. Technol. 53, 3718–3728.
Charbonnet, J.A., et al., 2022. Communicating confidence of per- and polyfluoroalkyl substance identification via high-resolution mass spectrometry. Environ. Sci. Technol. Lett. 9, 473–481.
D'Agostino, L.A., Mabury, S.A., 2014. Identification of novel fluorinated surfactants in aqueous film forming foams and commercial surfactant concentrates. Environ. Sci. Technol. 48, 121–129.
Kempisty, David, Racz, L., 2021. Forever Chemicals: Environmental, Economic, and Social Equity Concerns with PFAS in the Environment. CRC Press. https://doi.org/10.1201/9781003024521.
Dixit, F., et al., 2024. Closing PFAS analytical gaps: inter-method evaluation of total organofluorine techniques for AFFF-impacted water. J. Hazard. Mater. Lett. 5, 100122.
Dudášová, S., et al., 2024. An automated and high-throughput data processing workflow for PFAS identification in biota by direct infusion ultra-high resolution mass spectrometry. Anal. Bioanal. Chem. 416, 4833–4848.
Dwinandha, D., et al., 2023. Interpretable machine learning and reactomics assisted isotopically labeled FT-ICR-MS for exploring the reactivity and transformation of natural organic matter during ultraviolet photolysis. Environ. Sci. Technol. 58, 816–825.
Eeso, K., et al., 2023. Degradation of per- and polyfluoroalkyl substances in landfill leachate by a thin-water-film nonthermal plasma reactor. Waste Manag. 161, 104–115.
Guan, Y., et al., 2024. Near-complete destruction of PFAS in aqueous film-forming foam by integrated photo-electrochemical processes. Nat. Water 2, 443–452.
Koelmel, J.P., et al., 2022. FluoroMatch 2.0—Making automated and comprehensive non-targeted PFAS annotation a reality. Anal. Bioanal. Chem. 414, 1201–1215.
Kokoli, M., et al., 2023. Arena3Dweb: interactive 3D visualization of multilayered networks supporting multiple directional information channels, clustering analysis and application integration. NAR Genom. Bioinf. 5, 1–8.
Li, F., et al., 2020. Biomimetic degradability of linear perfluorooctanesulfonate (L-PFOS): degradation products and pathways. Chemosphere 259, 127502.
Li, K., et al., 2023a. Significantly accelerated photochemical perfluorooctanoic acid decomposition at the air–Water interface of microdroplets. Environ. Sci. Technol. 57, 21448–21458.
Li, Z.G., et al., 2023b. Generation mechanism of perfluorohexanesulfonic acid from polyfluoroalkyl sulfonamide derivatives during chloramination in drinking water. Environ. Sci. Technol. 57, 18462–18472.
Liu, J., et al., 2023. Comprehensive understanding of DOM reactivity in anaerobic fermentation of persulfate-pretreated sewage sludge via FT-ICR mass spectrometry and reactomics analysis. Water Res 229, 119488.
Liu, Z., et al., 2021. Near-quantitative defluorination of perfluorinated and fluorotelomer carboxylates and sulfonates with integrated oxidation and reduction. Environ. Sci. Technol. 55, 7052–7062.
Nguyen, T.V., et al., 2013. Rate laws and kinetic modeling of N-ethyl perfluorooctane sulfonamidoethanol (N-EtFOSE) transformation by hydroxyl radical in aqueous solution. Water Res 47, 2241–2250.
Qiao, B., et al., 2023. Nontarget screening and fate of emerging per- and polyfluoroalkyl substances in wastewater treatment plants in Tianjin. China. Environ. Sci. Technol. 57, 20127–20137.
Schymanski, E.L., et al., 2023. Per- and polyfluoroalkyl substances (PFAS) in PubChem: 7 million and growing. Environ. Sci. Technol. 57, 16918–16928.
Schymanski, E.L., et al., 2014. Strategies to characterize polar organic contamination in wastewater: exploring the capability of high resolution mass spectrometry. Environ. Sci. Technol. 48, 1811–1818.
Schymanski, E.L., Williams, A.J., 2017. Open science for identifying "Known unknown. Chemicals. Environ. Sci. Technol. 51, 5357–5359.
Singh, R.K., et al., 2019. Breakdown products from perfluorinated alkyl substances (PFAS) degradation in a plasma-based water treatment process. Environ. Sci. Technol. 53, 2731–2738.
Song, W., et al., 2024. Taming the unknown: advancing non-targeted analysis through collaborative data sharing and standardized data repositories. Environ. Sci. Technol. Lett.
Tachibana, K., et al., 2014. Reaction process of perfluorooctanesulfonic acid (PFOS) decomposed by DC plasma generated in argon gas bubbles. IEEE Trans. Plasma Sci. 42, 786–793.
Takeuchi, N., et al., 2014. Plasma–liquid interfacial reaction in decomposition of perfluoro surfactants. J. Phys. D. Appl. Phys. 47, 045203.
Tang, C., et al., 2023. Nontarget analysis and comprehensive characterization of iodinated polyfluoroalkyl acids in wastewater and river water by LC-HRMS with Cascade precursor-ion exclusions and algorithmic approach. Environ. Sci. Technol. 57, 17099–17109.
Taniyasu, S., et al., 2008. Analysis of trifluoroacetic acid and other short-chain perfluorinated acids (C_2–C_4) in precipitation by liquid chromatography–tandem mass spectrometry: comparison to patterns of long-chain perfluorinated acids (C_5–C_{18}). Anal. Chim. Acta 619, 221–230.
Trang, B., et al., 2022. Low-temperature mineralization of perfluorocarboxylic acids. Science 377, 839–845.
Vestergren, R., et al., 2024. A systematic workflow for compliance testing of emerging international classwide restrictions on PFAS. Environ. Sci. Technol.
Wang, D., et al., 2022. Influence of pulsed electric fields on photosynthesis in light/dark-acclimated lettuce. Agronomy 12, 173.
Wang, L., et al., 2024a. Deciphering microbe-mediated dissolved organic matter reactome in wastewater treatment plants using directed paired mass distance. Environ. Sci. Technol. 58, 739–750.
Wang, X., et al., 2024b. Machine learning–enhanced molecular network reveals global exposure to hundreds of unknown PFAS. Sci. Adv. 10, 1–12.
Wanzek, T., et al., 2024. A multiple lines of evidence approach to demonstrate effectiveness of PFAS remediation technologies. Groundw. Monit. Remediat. 44, 30–38.
Young, R.B., et al., 2022. PFAS analysis with ultrahigh resolution 21T FT-ICR MS: suspect and nontargeted screening with unrivaled mass resolving power and accuracy. Environ. Sci. Technol. 56, 2455–2465.
Yu, M., et al., 2019. Structure/reaction directed analysis for LC-MS based untargeted analysis. Anal. Chim. Acta 1050, 16–24.
Yu, M., Petrick, L., 2020. Untargeted high-resolution paired mass distance data mining for retrieving general chemical relationships. Commun. Chem. 3, 1–6.
Yu, N., et al., 2018. Non-target and suspect screening of per- and polyfluoroalkyl substances in airborne particulate matter in China. Environ. Sci. Technol. 52, 8205–8214.
Zhang, H., et al., 2024. Removal of per- and polyfluoroalkyl substances from water by plasma treatment: insights into structural effects and underlying mechanisms. Water Res. 253, 121316.
Zhou, Z., et al., 2023. Complementary elucidation of the molecular characteristics of groundwater dissolved organic matter using ultrahigh-resolution mass spectrometry coupled with negative- and positive-ion electrospray ionization. Environ. Sci. Technol. 57, 4690–4700.
Zhu, B., et al., 2019. Occurrence and degradation potential of fluoroalkylsilane substances as precursors of perfluoroalkyl carboxylic acids. Environ. Sci. Technol. 53, 4823–4831.
Zweigle, J., et al., 2023. PFAS-contaminated soil site in Germany: nontarget screening before and after direct TOP assay by Kendrick Mass Defect and FindPFΔS. Environ. Sci. Technol. 57, 6647–6655.
Zweigle, J., et al., 2022. FindPF?S: non-target screening for PFAS-comprehensive data mining for MS²fragment mass differences. Anal. Chem. 94, 10788–10796.